

## EFFECTS OF HORIZONTAL SHEAR OF VERTICAL VELOCITY IN DBS AND SA MEAN WIND ESTIMATES REVEALED BY A COMBINATION OF LES AND VIRTUAL RADAR

D. E. Scipión<sup>1,3,\*</sup>, R. D. Palmer<sup>2,3</sup>, P. B. Chilson<sup>2,3</sup>, E. Fedorovich<sup>2</sup>, R. J. Doviak<sup>4</sup>, G. Zhang<sup>2,3</sup>, A. M. Botnick<sup>2</sup>

<sup>1</sup>School of Electrical and Computer Engineering, University of Oklahoma, Norman, Oklahoma, USA

<sup>2</sup>School of Meteorology, University of Oklahoma, Norman, Oklahoma, USA

<sup>3</sup>Atmospheric Radar Research Center, University of Oklahoma, Norman, Oklahoma, USA

<sup>4</sup>National Severe Storms Laboratory, Norman, Oklahoma, USA

### Abstract

The two techniques most often used to retrieve the three-dimensional wind (zonal, meridional, and vertical) from wind profiling radars are Doppler Beam Swinging (DBS) and Spaced Antenna (SA). These well-known techniques are based on the assumption of homogeneity across the region defined by the radar beam directions. However, this assumption is not always valid due to the presence of spatial inhomogeneities in the wind field and shear. The SA method incorporates only a vertical beam for transmission. The backscattered signal is then received using spatially separated antennas. As a result, the SA technique relies less heavily on spatial homogeneity compared to DBS. However, SA could be more sensitive to vertical velocity variations, especially in active convective boundary layer cases. In DBS, the time needed to complete a typical DBS scan can also make temporal variability a concern, which is often on the order of a few minutes.

The present study employs a combination of a virtual radar and Large-Eddy Simulations (LES) in order to evaluate different wind-profiling radar methods of estimating wind in the presence of horizontal shear of vertical velocity. Measurements from DBS are compared with those from SA. For this study, the DBS method was configured for five beam directions (each with a beam width of 9 degrees) in the four cardinal directions with a zenith angle of 15.5 degrees and a vertical beam. Dwell time for each beam was set to 30 s, producing a revisit time of 2.5 min. The SA method was designed with three receivers: one located at the center of the LES sub-domain, the others 1 m to the zonal and meridional directions, respectively. The SA dwell time is set to 60 s. Results from both DBS and SA were compared to the "true" fields obtained directly from the LES.

---

\* Corresponding author address: Danny E. Scipión, University of Oklahoma, School of Meteorology, 120 David L. Boren Blvd., Rm 5900, Norman, OK 73072-7307; e-mail: dscipion@ou.edu

### 1. INTRODUCTION

Boundary layer radars (BLR) are widely used to study and monitor the lower atmosphere [e.g., Angevine et al., 1994; Angevine, 1999; Cohn and Angevine, 2000; Grimsdell and Angevine, 2002; Scipión et al., 2008]. Profiles of the wind vector directly above the instrument are obtained using the DBS method [Balsley and Gage, 1982]. The BLR can be used to study the boundary layer under a wide variety of meteorological conditions, which has been proven invaluable for such investigations [e.g., Rogers et al., 1993; Angevine et al., 1994; Wilczak et al., 1996; Dabberdt et al., 2004].

SA is another technique [Briggs and ad D. H. Shinn, 1950] that has been used to obtain wind profiles and turbulence in the boundary layer [Cohn et al., 2001]. If the wind is uniform, SA can measure the cross-beam wind, as well as the radial wind component within the radar resolution volume [Doviak and Zrnić, 2006; Zhang and Doviak, 2007]. The Full Correlation Analysis (FCA) method was introduced by Briggs [1984] as a technique which uses both the auto- and cross-correlation functions to estimate wind. SA systems are used to infer the motion and changes of the diffraction pattern and are used to estimate the parameters of the laminar and/or turbulent flow advecting a multitude of scatterers assumed to be uniformly distributed throughout the radar's resolution volume [Holloway et al., 1997].

A different method to estimate the cross-beam wind is presented in Doviak et al. [1996]; Holloway et al. [1997] which also uses the auto- and cross-correlation function. None of the methods [Briggs, 1984; Doviak et al., 1996] considers the effects of shear on the cross-beam wind estimates. A new approach was presented in Zhang and Doviak [2007] which includes this effect in their formulation.

A realistic case is considered that incorporates all typical forcings that drive a daytime clear CBL [Botnick and Fedorovich, 2008]. Flow structure for this CBL case is investigated through both real radar measurements and

numerical simulations. Numerically generated, CBL flow fields are employed in two ways. First, they are used to emulate a virtual BLR along the lines discussed in Muschinski et al. [1999] and Scipi3n et al. [2008]. Second, they represent a source of reference information about the CBL turbulent flow.

The setup for the study includes the simulation of two different kinds of radars. One includes a conventional setup used to retrieve winds using DBS, and it consists of one single radar pointing in five non-coplanar directions. The second emulates the SA setup with three receivers to obtain the cross-beam wind in the zonal and meridional directions. For the DBS setup, the three wind components are obtained through application of the technique presented in Balsley and Gage [1982]. The wind components from SA are obtained after applying the method presented in Doviak et al. [1996] and Holloway et al. [1997].

This paper is organized as follows. In Section 2, the main features of the LES code employed in this study are briefly described with a focus on recently implemented features and methodologies of using LES for CBL flow data generation. Theoretical derivations of the shear effects in the wind estimation techniques, DBS and SA, are presented in Section 3. The virtual radar is presented in Section 4 along with the radar experimental setup and some modifications for the SA radar. Section 5 discusses comparisons of wind fields and horizontal shear of vertical velocity obtained by different techniques. Finally, in Section 6, conclusions are summarized and directions of future work are outlined.

## 2. LARGE EDDY SIMULATIONS (LES)

The main features of the LES code employed in our study are described by Fedorovich et al. [2004a,b] and Conzemius and Fedorovich [2006]. Over the last two years, the code has undergone several revisions aimed at improving its numerical accuracy and the ability to perform in realistic atmospheric environments. Simulation initialization procedures were modified to incorporate realistic atmospheric sounding data which was retrieved from observations or from larger-scale atmospheric model/analysis outputs [Botnick and Fedorovich, 2008]. The LES was applied to reproduce a daytime CBL case observed at the Southern Great Plains Atmospheric Radiation Measurement Climate Research Facility (SGP ACRF) in Lamont, Oklahoma, on June 8 2007. A sub-set of the LES output was employed as an input data set for the virtual BLR. The BLR sub-domain had spatial limits of  $1860 \text{ m} \leq X \leq 3260 \text{ m}$ ,  $1860 \text{ m} \leq Y \leq 3260 \text{ m}$ , and  $0 \text{ m} \leq Z \leq 2000 \text{ m}$ . The BLR

used three-dimensional fields of potential temperature  $\Theta$ , specific humidity  $q$ , flow velocity components  $u$ ,  $v$ , and  $w$  along the coordinate directions  $x$ ,  $y$ , and  $z$ , respectively, and sub-grid TKE  $E$ . A snapshot of the simulated CBL flow structure is given in Figure 1.

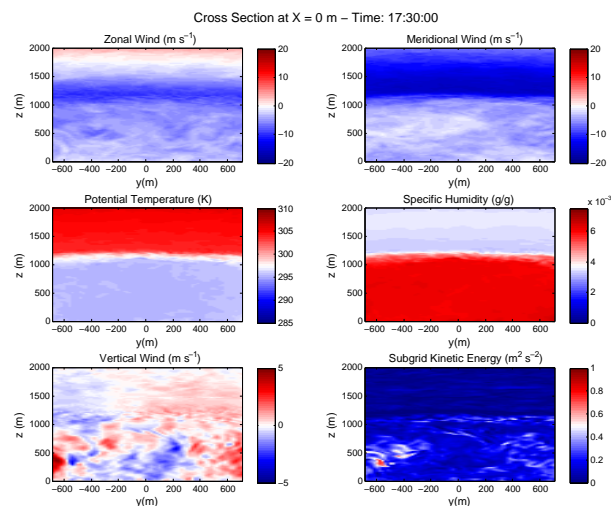


Figure 1: Examples of LES output fields in the sub-domain of the radar simulator. Top-left: zonal wind. Top-right: meridional wind. Middle-left: vertical velocity. Middle-right: potential temperature. Bottom-left: specific humidity. Bottom-right: sub-grid kinetic energy. All data presented refer to the same single realization in time (one LES time step).

By its nature, the clear atmospheric CBL is a turbulent boundary layer, whose turbulence is primarily forced by heating from the underlying surface. Another characteristic feature of the CBL flow is its coherent structure on larger scales that is represented by convective updrafts (thermals) and downdrafts which are clearly observed in the vertical velocity field pattern (see Fig. 2).

## 3. SHEAR EFFECTS

### 3.1. Doppler Beam Swinging

Usually, the calculations of DBS winds are under the strict assumption that the three wind components are constant across the region defined by the beam locations. However, if we consider that only the vertical velocity assumption does not hold and introducing the horizontal components of the vertical velocity shear, we can

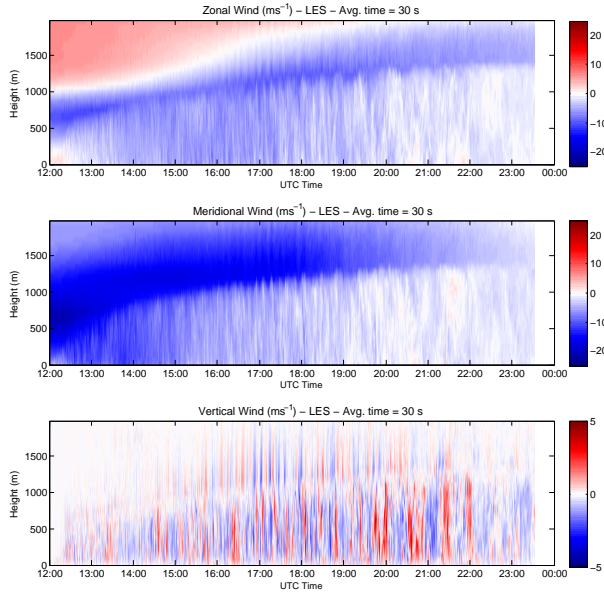


Figure 2: Vertical profile of the LES winds (zonal, meridional, and vertical) located at the center of the domain. The integration time for each of the wind components is 30 s.

write the equation for any oblique beam as:

$$V_r = u_o \sin \theta \sin \phi + v_o \sin \theta \cos \phi + \tilde{w} \cos \theta, \quad (1)$$

$$\tilde{w} = w_o + s_u z_o \tan \theta \sin \phi + s_v z_o \tan \theta \cos \phi, \quad (2)$$

$$s_u = \frac{\tilde{w} - w_o}{z_o \tan \theta}, \quad \phi = 90^\circ, \quad (3)$$

$$s_v = \frac{\tilde{w} - w_o}{z_o \tan \theta}, \quad \phi = 0^\circ, \quad (4)$$

where  $u_o$ ,  $v_o$ , and  $w_o$  are the zonal, meridional, and vertical mean wind flow;  $\theta$  and  $\phi$  are the zenith and azimuth angles respectively;  $z_o$  is the vertical range where the radial velocity is calculated;  $\tilde{w}$  is the true vertical velocity at the beam position; finally,  $s_u$  and  $s_v$  represent the horizontal shear components of the vertical velocity caused by the horizontal gradient in the true vertical velocity ( $\tilde{w}$ ) and the assumed constant mean vertical wind ( $w_o$ ) within the volume defined by all the beams.

Regrouping terms can lead to a more known expression for the radial velocity:

$$V_r = (u_o + s_u z_o) \sin \theta \sin \phi + (v_o + s_v z_o) \sin \theta \cos \phi + w_o \cos \theta \quad (5)$$

$$\tilde{V}_r = \tilde{u} \sin \theta \sin \phi + \tilde{v} \sin \theta \cos \phi + w_o \cos \theta, \quad (6)$$

where  $\tilde{u} = u_o + s_u z_o$  and  $\tilde{v} = v_o + s_v z_o$  are the DBS-measured zonal and meridional wind biased by the hor-

izontal shear of the vertical wind in the  $x$  and  $y$  direction [Zhang and Doviak, 2007]. The solution to the set of equations (multiple beams) shows that the horizontal shear effect caused by the vertical velocity can not be separated from the horizontal wind estimates.

### 3.2. Spaced Antenna

In Zhang and Doviak [2007], the generalized theoretical expression for the cross-correlation for spaced antenna wind profilers is presented. However, the equation had been derived for a horizontal pointing weather radar, and needs to be adapted for a vertically pointing wind profiler in the same fashion it is presented in Doviak et al. [1996] and Holloway et al. [1997]. The modified equation is presented in below:

$$c_{12}(\tau) = \exp(-2jk_o w_o \tau - 2k_o^2(\sigma_R^2 s_w^2 - \sigma_t^2)\tau^2 - \beta_h^2((u_o + s_u z_o)\tau - \Delta x/2)^2 - \beta_h^2((v_o + s_v z_o)\tau - \Delta y/2)^2), \quad (7)$$

where  $\tau$  represents the time lag,  $k_o = 2\pi/\lambda$  is the radar wavenumber,  $\lambda$  is the radar wavelength, and  $\Delta x$  and  $\Delta y$  represent the separation of the two receivers along the  $x$  and  $y$  direction, respectively.  $\sigma_t$  is the root-mean-square error (rms) wind variability of each wind component for isotropic turbulence,  $\sigma_R$  is the second central moment of the range weighting function assumed to be equal for both receivers,  $\beta_h$  is related to the scale length of the diffraction pattern (see equations 3, 4, 5, and 6 of Holloway et al. [1997]), and  $u_o$ ,  $v_o$ , and  $w_o$  are the three wind components. Finally,  $s_u$ ,  $s_v$ , and  $s_w$  are the three components of the vertical velocity shear. The effects of the vertical wind  $w_o$  and vertical shear  $s_w$  are typically small and will be omitted in the future [Holloway et al., 1997; Zhang and Doviak, 2007].

Taking the magnitude of (7) and rewriting in a more convenient form, we obtain the normalized autocorrelation ( $\Delta x, \Delta y = 0$ ) and cross-correlation functions for receiving antenna separations less than the width of the transmitter's antenna beam at the range of interest:

$$|c_{11}(\tau)| = \exp[-\beta_h^2(\tilde{u}^2 + \tilde{v}^2) - 2k_o^2 \sigma_t^2 \tau^2] + \frac{N}{S} \delta(\tau) \quad (8)$$

$$|c_{12}(\tau)| = \exp[-\beta_h^2(\tilde{u}\tau - \Delta x/2)^2 - \beta_h^2 \tilde{v}^2 \tau^2 - 2k_o^2 \sigma_t^2 \tau^2], \quad (9)$$

where  $S$  is the signal power,  $N$  is the receiver noise power,  $\delta(\tau)$  is the Dirac delta function, and  $\tilde{u} = u_o + s_u z_o$  and  $\tilde{v} = v_o + s_v z_o$  are the SA measured wind components in the  $x$  and  $y$  direction, in other words, the

baseline wind biased by the baseline shear [Zhang and Doviak, 2007].

Equations 8 and 9 are the same as the ones presented in Holloway et al. [1997], and are used to estimate the measured wind and turbulence. Once again, it is clear that it is impossible to separate the horizontal shear component of the vertical velocity from the measured wind, and if significantly large, the estimates of the horizontal wind will be erroneous.

## 4. EXPERIMENTAL CONFIGURATIONS

### 4.1. DBS Configuration

The method used to emulate the virtual radar signal within the atmospheric flow fields generated by LES is described by Scipi3n et al. [2008] and is based on the work of Muschinski et al. [1999]. The time-series data for the virtual BLR are created by summing the contribution from each LES point within the radar resolution volume which is defined by the radar pulse width and beam width. The virtual radar is patterned after a Vaisala UHF BLR-LAP3000 and operates at a central frequency of 915 MHz, with a two-way half-power beam width of 9°. It is possible to direct the radar beam vertically or electronically steer it at 15.5° off-vertical along 4 different azimuth angles: 0°, 90°, 180°, 270°.

In the present study, a range resolution of 60 m is used. Additive white Gaussian noise, corresponding to a signal-to-noise ratio (SNR) of 5 dB, was added to the time-series data to produce more realistic signals. The three spectral moments (power, mean radial velocity, and spectral width) are estimated after conventional spectral analysis of the time-series data. The maximum time period for this case was ~11.5 hr. Radial velocities were later used to estimate the wind components using DBS.

### 4.2. SA Configuration

The radar simulator for this study was developed following the procedure described in the section 4.1; however, a few modifications are required for simulation of the SA receiver signals. The signal amplitude in the simulator after time  $\tau$  is proportional to  $C_n^2$  and inversely proportional to  $r_0^2$ , which is the range of the center of the sampling volume. The phase difference is proportional to the

velocity vector according to

$$V(t_0 + \tau) = A' \sum_{p=1}^N \sqrt{C_n^2(t_0 + \tau)^{(p)} W_r^{(p)} W_b^{(p)}} \cdot \exp[-j(\varphi_0^{(p)} + k_0(r_{tx}^{(p)} + r_{rx}^{(p)} + k_0(\hat{\mathbf{e}}_{tx}^{(p)} + \hat{\mathbf{e}}_{rx}^{(p)}) \cdot \mathbf{v}^{(p)}(t_0 + \tau)\tau)], \quad (10)$$

$$A' = \frac{G}{\lambda r_0^2} \sqrt{0.0330 k_B^{-11/6}}, \quad (11)$$

where  $p$  represents each individual grid point of the  $N$  points contained within the resolution volume,  $G$  is a constant proportional to the power transmitted and gain of the transmitter and receiver,  $\varphi_0^{(p)}$  is a random initial phase,  $k_0$  is the radar wavenumber,  $\hat{\mathbf{e}}_{tx}^{(p)}$  is the unit vector directed from the transmitter antenna to the  $p^{th}$  LES grid cell,  $\hat{\mathbf{e}}_{rx}^{(p)}$  is the unit vector directed from the receiver antenna to the  $p^{th}$  LES grid cell,  $\mathbf{v}^{(p)}$  is the instantaneous radial velocity, and  $k_B$  is the Bragg wavenumber ( $k_B = \frac{4\pi}{\lambda}$ ).  $W_r$  represents the range weighting function [Holdsworth and Reid, 1995; Scipi3n et al., 2008]. Finally,  $W_b$  is the beam-pattern weighting function [Yu, 2000; Cheong et al., 2004; Scipi3n et al., 2008].

Three spaced receivers were used to estimate the zonal and meridional wind. One was located at the center of the BLR sub-domain, and the other two were located at 1 m to the north and east directions. This configuration is very helpful in the determination of the horizontal wind components along each baseline. As in the DBS configuration, the range resolution is 60 m and the additive Gaussian noise was added with an SNR of 5 dB to generate realistic signals. The techniques used to obtain the horizontal wind are presented in equations 41, 42, and 43 in Holloway et al. [1997]. All the techniques showed similar results, so it was not possible to choose any of the techniques over the others. The technique chosen was the fitted Gaussian parameters applied to the log of the ratio between the cross- and auto-correlation functions (SLR), with  $a_n = 1.61$  (equation 42 in Holloway et al. [1997]). The dwell time chosen to obtain the SA wind estimates was 60 s. Later, the 60 s estimates were averaged to obtain the desired estimates (300 s in this case).

## 5. RESULTS

The estimates from the horizontal wind ( $u$  and  $v$ ) were analyzed for three different quantities: resolved LES values along a vertical profile at the center the simulation domain (LES), DBS estimates calculated from the radial velocities of the virtual BLR pointing in the five directions (DBS), and SA estimates calculated from the three

spaced receivers auto- and cross-correlation functions (SA). The averaging time chosen for all the estimates is 5 min.

To obtain the DBS values, the following procedure was used. First, radial velocities from each of the five virtual BLR beams were estimated with a dwell time of 30 s. Second, velocity samples were computed every 2.5 min representing the DBS sampling time. Third, the DBS technique was used to retrieve the three wind components. Finally, the wind components were averaged over 5-min. The LES data were averaged in time to obtain the 5-min estimates used for comparison. Estimates from SA are calculated every 60 s. Wind estimates from SA were averaged over the same time period.

Values of the two wind components ( $u$  and  $v$ ) obtained by different techniques are presented in Figures 3 (zonal) and 4 (meridional). Estimates from DBS and SA do not appear to be as smooth as those from LES, which is primarily due to the shear effect described in Section 3. Other causes for the discrepancies are the realistic noise contamination and associated measurement error. For SA estimates, it is clear that the technique can not resolve the first three heights due to a lack of LES grid points within the resolution volume. In the following analysis, these three heights are removed. The bias error in both wind estimates (zonal and meridional) is analyzed in more detail for each of the techniques.

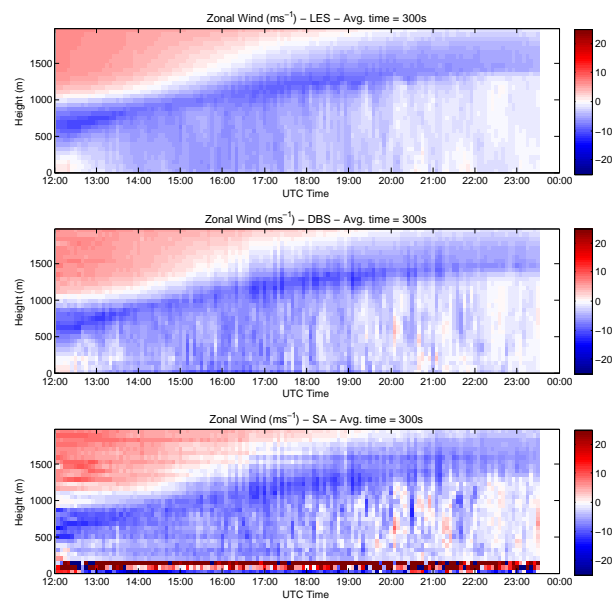


Figure 3: Zonal wind estimates averaged for 5 min. Top: LES-Profile at the center of the domain. Middle: DBS estimates with a dwell time of 30 s and a revisit time of 2.5 min. Bottom: SA estimates with a dwell time of 60 s.

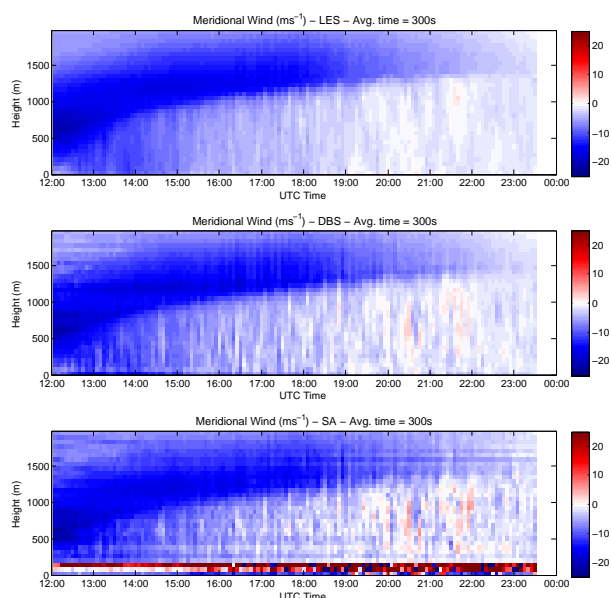


Figure 4: Meridional wind estimates averaged for 5 min. Top: LES-Profile at the center of the domain. Middle: DBS estimates with a dwell time of 30 s and a revisit time of 2.5 min. Bottom: SA estimates with a dwell time of 60 s.

The DBS error estimates are presented in Figure 5, where the zonal and meridional estimates are plotted versus their corresponding LES estimates. There is good agreement between both estimates. After plotting the difference between the DBS and LES wind estimates (bias error) as a function of wind speed, it is clear from the plot that the larger errors occur at lower wind speeds. In this CBL case, these velocities are located within the mixed layer where the strong updrafts and downdrafts occur (see vertical velocity in Fig. 2) and cause a strong horizontal shear of vertical velocity effect in the zonal and meridional wind estimates.

According to the theory presented in Section 3, the main cause of this bias error is the horizontal shear of the vertical velocity [Zhang and Doviak, 2007]. In realistic measurements, it is impossible to separate this effect from the real wind estimates, and/or to evaluate this quantity. In this unique situation, the “true” vertical wind ( $\bar{w}$ ) at each beam direction had been recorded directly from the LES vertical wind field. The resultant horizontal shear of the vertical velocity is calculated at each LES step (1 s) using equations 3 and 4, averaged in time to obtain the 5-min estimates, interpolated at each height, and presented in panels middle-top and bottom panels of Figure 6 for the zonal and meridional components, respectively.

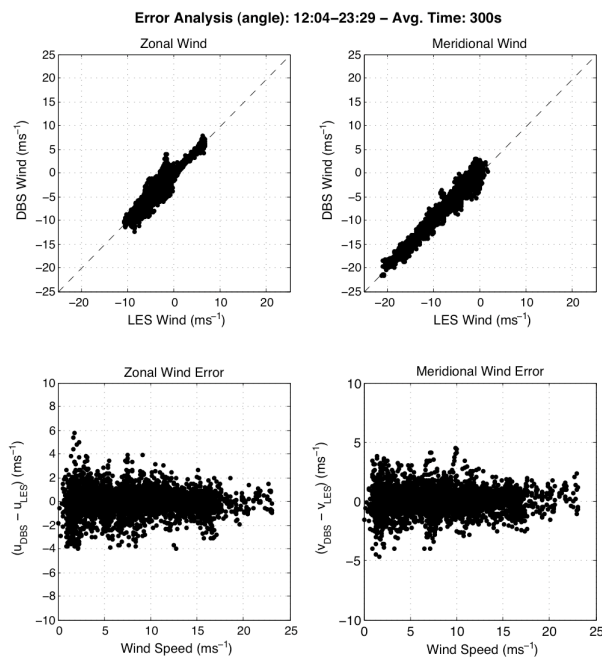


Figure 5: Error analysis of the DBS estimates. Top-left: zonal wind comparison between DBS and LES. Top-right: meridional wind comparison between DBS and LES. Bottom-left: zonal wind error vs. wind speed. Bottom-right: meridional wind error vs. wind speed.

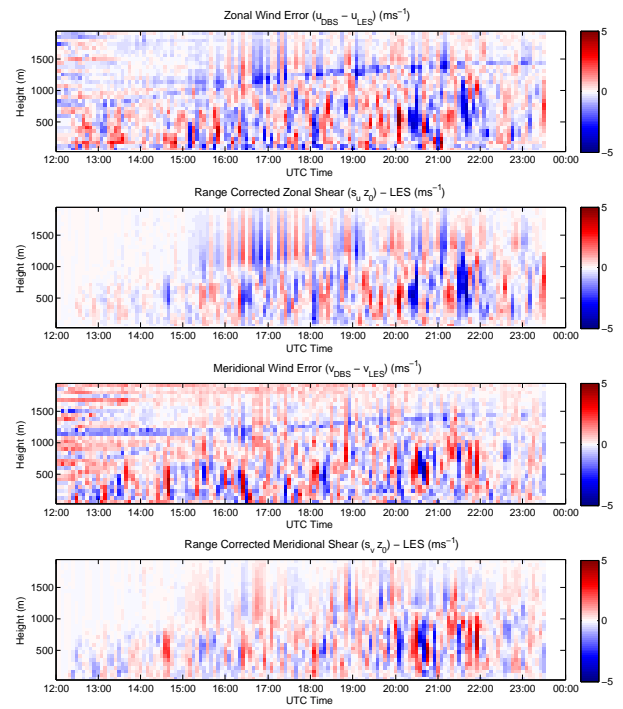


Figure 6: Error analysis as a function of time. Top: zonal wind error from DBS estimates. Middle-top: range corrected zonal shear from LES. Middle-bottom: meridional wind error from DBS estimates. Bottom: range corrected meridional shear from LES.

From the plot, it is clear that there is good correlation between the bias error in the zonal and meridional estimates and the horizontal shear of the vertical velocity. There are some other features that need to be mentioned. In the theoretical calculations, especially at the beginning of the simulation, the shear effect is not present above the BL top. However, there is still some bias noticeable in the zonal and meridional bias error. This might be an overestimation of the wind component due to inhomogeneities within the volume that encloses the five DBS beams [Cheong et al., 2008]. There is also a clear indication of the vertical shear of the horizontal wind located at almost the same height of the BL top; graphically, it can be identified as the “blue” band located at approximately 1000 m.

The bias error is now analyzed as a function of height and is compared with horizontal shear of the vertical velocity (see Fig. 7). As expected, the larger errors occur at lower heights (within the CBL) where strong updrafts and mild downdrafts are present. This zone is characterized with strong horizontal shear caused by vertical velocity. This effect is observed clearly in both wind components (zonal and meridional). There is good correlation between the biased error and the range corrected horizontal shear (see bottom panels).

As in the case of DBS, the bias error is analyzed for the SA technique. The comparison between the zonal and meridional wind estimates from SA and LES are presented in Figure 8. In general, the estimates agree well, but are more spread out than those of DBS. The same widening in the spread is observed when the biased error is plotted as a function of wind speed (bottom). It is again clear that the larger errors occur at lower wind speeds. Again, lower horizontal wind speeds are present within the mixed layer of the CBL. It is also noticeable (especially in the zonal wind bias error) that at about  $18 \text{ m s}^{-1}$  the bias error is reduced drastically, an indication of strong winds above the BL top.

The bias error is now plotted as a function of height for the entire simulation and compared with the theoretical horizontal shear of the vertical velocity (see Fig. 9). Calculations of the theoretical shear vary from those of DBS. In this case, the shear is calculated inside the resolution volume as the average of the gradients of the vertical velocities along the  $x$  and  $y$  directions. The theoretical shear is presented in Figure 9 for the zonal (middle-top) and meridional (bottom) wind components. Again, there is a correlation between the bias error and the horizontal shear of the vertical velocity. However, there are clearly other factors that contribute to this bias in the SA wind estimates, needing further analysis.

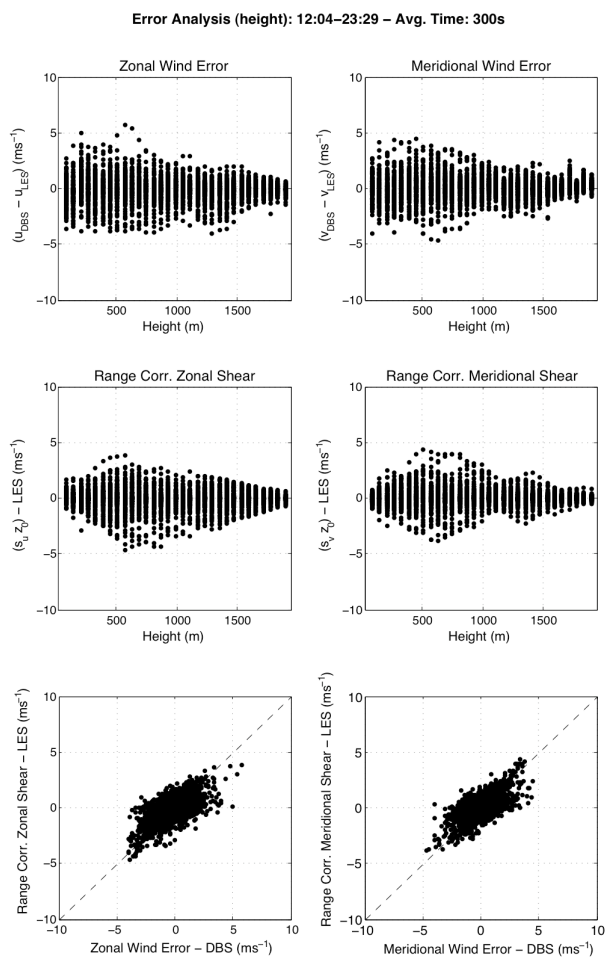


Figure 7: Error analysis of the DBS estimates as a function of height. Top-left: zonal error. Top-right: meridional error. Middle-left: range corrected zonal shear from LES. Middle-right: range corrected meridional shear from LES. Bottom-left: zonal wind error vs. range corrected zonal shear. Bottom-right: meridional wind error vs. range corrected meridional shear.

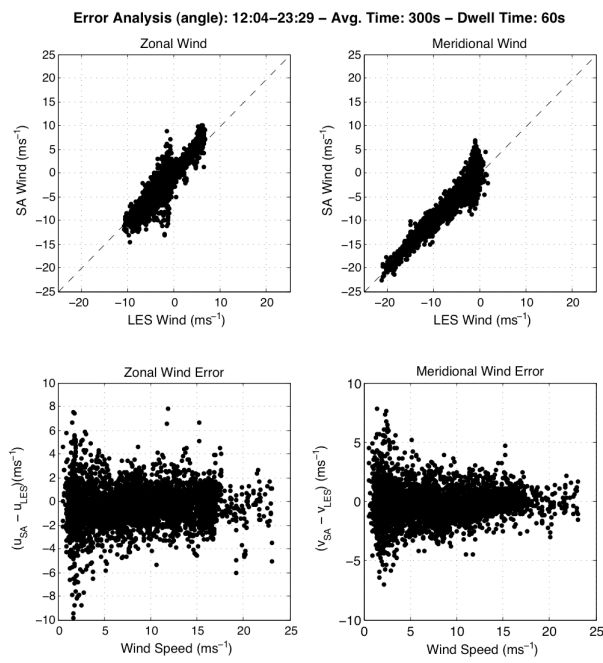


Figure 8: Error analysis of the SA estimates. Top-left: zonal wind comparison between SA and LES. Top-right: meridional wind comparison between SA and LES. Bottom-left: zonal wind error vs. wind speed. Bottom-right: meridional wind error vs. wind speed.

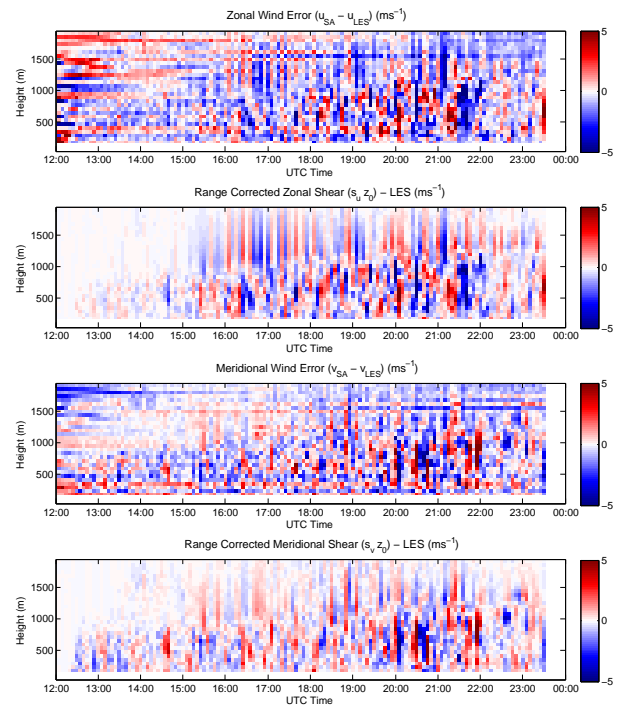


Figure 9: Error analysis as a function of time. Top: zonal wind error from SA estimates. Middle-top: range corrected zonal shear from LES. Middle-bottom: meridional wind error from SA estimates. Bottom: range corrected meridional shear from LES

The error and the range corrected shear are now plotted as a function of height in Figure 10. As the DBS case, the major error is located at lower heights (within the CBL). However, the spread is wider than the DBS estimates (measurements and theoretic). Finally, a scatter plot of both quantities is presented in which the correlation between them is clearly present.

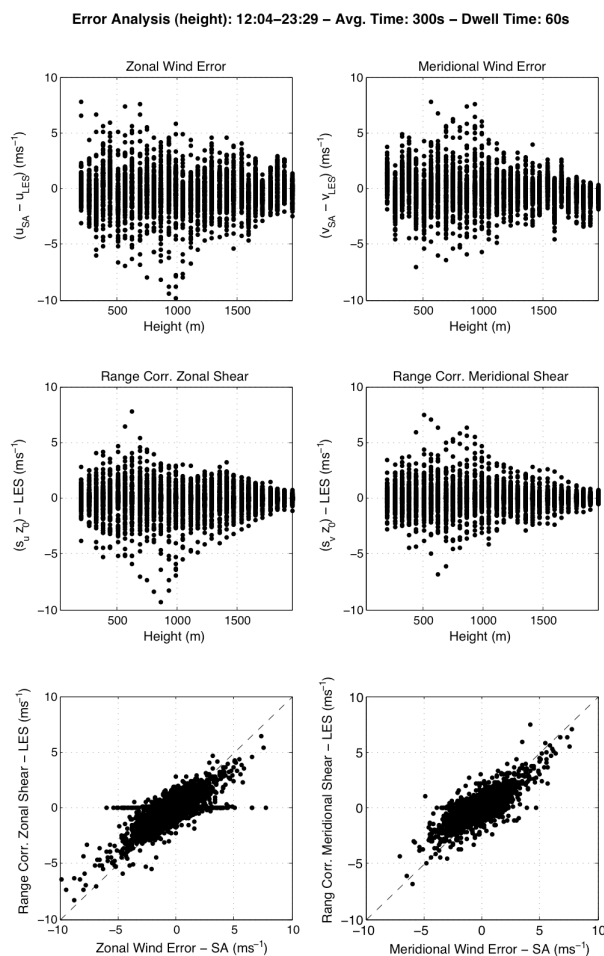


Figure 10: Error analysis of the SA estimates as a function of height. Top-left: zonal error. Top-right: meridional error. Middle-left: range corrected zonal shear from LES. Middle-right: range corrected meridional shear from LES. Bottom-left: zonal wind error vs. range corrected zonal shear. Bottom-right: meridional wind error vs. range corrected meridional shear.

## 6. CONCLUSIONS

Comparison of the virtual BLR estimates of three-dimensional winds obtained with two techniques (DBS and SA) have been presented. A modification of the vir-

tual boundary layer radar is also included for the simulation of the SA receiver signals based on LES. The LES was initialized with the CBL case observed on the U. S. Central Plains on June 8, 2007. There is reasonable agreement between the zonal and meridional estimates from SA and DBS. These quantities are also compared with a vertical profile of the wind fields located at the center of the LES sub-domain, which is collocated with the virtual radars. The LES profiles are considered as ground “truth”, and are used as a reference for comparison.

Usually, the bias in the DBS estimates is attributed to the presence of inhomogeneities within the volume encompassed by the beams. This effect is also reduced if the number of beams and the averaging time is increased [Cheong et al., 2008]. If the only effect that causes discrepancies in the estimates are inhomogeneities, the SA technique would have better estimates than DBS because it relies less on the homogeneity assumption due to the close proximity of the receivers and narrowness of antenna beam patterns. However, the results presented show that the SA estimates are worse than the DBS estimates in the zonal and meridional component.

After deeper investigation of the results, it was found that the main cause of the discrepancies or bias error in the DBS and SA compared with LES are due to the presence of horizontal shear of the vertical velocity.

This shear affects both techniques differently. The derivation of the shear effect in DBS estimates is presented in Section 3.1. In SA, the theoretical shear was adapted from the work of Zhang and Doviak [2007] and presented in Section 3.2. The DBS uses oblique beams in the estimation of horizontal winds. The projection of the vertical beam shear within the oblique beams depends on the zenith angle. The bigger the angle the lower the influence of the shear in the estimates of the wind. This is probably the main cause of the lower bias error in DBS than in SA.

The good agreement between the bias error of the zonal and meridional winds and the theoretical range corrected horizontal shear of the vertical velocity for both techniques supports that the theory is correct. In active CBL cases, the error can be more than 400%, especially within the mixed layer (see Figs. 5 and 6: bottom).

Another factor that contributed to an increase in the bias error is the vertical shear of the horizontal wind that can be clearly observed in the DBS estimates. This requires further analysis. Also, there are some other causes of error in the SA estimates which need theoretical formulation. These causes will be addressed in future work.

## ACKNOWLEDGMENTS

Support for this work was provided by the National Science Foundation under Grant No. 0553345.

## References

- Angevine, W. M., 1999: Entrainment results with advection and case studies from Flatland boundary layer experiments. *J. Geophys. Res.*, **104**, 30947–30963.
- Angevine, W. M., A. B. White, and S. K. Avery, 1994: Boundary-layer depth and entrainment zone characterization with a boundary-layer profiler. *Boundary-Layer Meteorol.*, **68**, 375–385.
- Balsley, B. B., and K. Gage, 1982: On the use of radars for operational profiling. *Bull. Amer. Meteor. Soc.*, **63**, 1009–1018.
- Botnick, A. M., and E. Fedorovich, 2008: Large eddy simulation of atmospheric convective boundary layer with realistic environmental forcings. *Quality and Reliability of Large-Eddy Simulations*, J. Meyers et. al., Eds., Springer, 193 – 204.
- Briggs, B., 1984: *The analysis of spaced sensor records by correlation techniques*. Vol. 13 of *Handbook for MAP*, pp. 166 – 186. SCOSTEP Secretariat, University of Illinois, Urbana, IL.
- Briggs, B., and G. J. P. and D. H. Shinn, 1950: The analysis of observation on spaced receivers of the fading radio signals. *Proc. Phys. Soc. London Sect. B.*, **63**, 106 – 121.
- Cheong, B. L., M. W. Hoffman, and R. D. Palmer, 2004: Efficient atmospheric simulation for high-resolution radar imaging application. *J. Atmos. Oceanic Technol.*, **21**, 374–378.
- Cheong, B. L., T.-Y. Yu, R. D. Palmer, K.-F. Yang, M. W. Hoffman, S. J. Frasier, and F. J. Lopez-Dekker, 2008: Effects of Wind Fields Inhomogeneities of Doppler Beam Swinging Revealed by an Imaging Radar. *J. Atmos. Oceanic Technol.*, **25**, 1414 – 1422.
- Cohn, S. A., and W. M. Angevine, 2000: Boundary level height and entrainment zone thickness measured by lidars and wind-profiling radars. *J. Appl. Meteorol.*, **39**, 1233–1247.
- Cohn, S. A., W. O. J. Brown, C. L. Martin, M. S. Susedik, G. Maclean, and D. B. Parsons, 2001: Clear air boundary layer spaced antenna wind measurements with the Multiple Antenna Profiler MAPR. *Ann. Geophys.*, **19**(845 – 854).
- Conzemius, R. J., and E. Fedorovich, 2006: Dynamics of sheared convective boundary layer entrainment. Part I: Meteorological background and large-eddy simulations. *J. Atmos. Sci.*, **63**, 1151–1178.
- Dabberdt, W. F., G. L. Frederick, R. M. Hardesty, W. C. Lee, and K. Underwood, 2004: Advances in meteorological instrumentation for air quality and emergency response. *Meteor. Atm. Phys.*, **87**, 57–88.
- Doviak, R. J., R. J. Latatits, and C. L. Holloway, 1996: Cross correlations and cross spectra for spaced antenna wind profilers. 1. Theoretical analysis. *Radio Sci.*, **31**(1), 157 – 180.
- Doviak, R. J., and D. S. Zrnić, 2006: *Doppler Radar and Weather Observations*. Dover.
- Durrant, D. R., 1999: *Numerical methods for wave equations in geophysical fluid dynamics*. Springer-Verlag New York, Inc.
- Ecklund, W. L., K. S. Gage, and C. R. Williams, 1995: Tropical precipitation studies using a 915-MHz wind profiler. *Radio Sci.*, **30**, 1055–1064.
- Fedorovich, E., and R. Conzemius, 2008: Effects of wind shear on the atmospheric convective boundary layer structure and evolution. *Acta Geophysica*, **56**, 114 – 141.
- Fedorovich, E., R. Conzemius, I. Esau, F. K. Chow, D. Lewellen, C.-H. Moeng, D. Pino, P. Sullivan, and J. V.-G. de Arellano, 2004a: Entrainment into sheared convective boundary layers as predicted by different large eddy simulation codes. in *Preprints, 16th Symp. on Boundary Layers and Turbulence, Amer. Meteor. Soc., 9-13 August, Portland, Maine, USA*, pp. CD-ROM, P4.7.
- Fedorovich, E., R. Conzemius, and D. Mironov, 2004b: Convective entrainment into a shear-free linearly stratified atmosphere: Bulk models re-evaluated through large-eddy simulations. *J. Atmos. Sci.*, **61**, 281–295.
- Gage, K. S., C. R. Williams, and W. L. Ecklund, 1994: UHF wind profilers: A new tool for diagnosing and classifying tropical cloud systems. *Bull. Amer. Meteor. Soc.*, **75**, 2289–2294.
- Grimsdell, A. W., and W. M. Angevine, 2002: Observation of the afternoon transition of the convective boundary layer. *J. Appl. Meteorol.*, **41**, 3–11.
- Holdsworth, D. A., and I. M. Reid, 1995: A simple model of atmospheric radar backscatter: Description and application to the full correlation analysis of spaced antenna data. *Radio Sci.*, **30**, 1263–1280.

- Holloway, C. L., R. J. Doviak, S. A. Cohn, R. J. Latatits, and J. S. V. Baelen, 1997: Cross correlations and cross spectra for spaced antenna wind profilers. 2. Algorithms to estimate wind and turbulence. *Radio Sci.*, **32**(3), 967–982.
- Muschinski, A. P., P. P. Sullivan, R. J. Hill, S. A. Cohn, D. H. Lenschow, and R. J. Doviak, 1999: First synthesis of wind-profiler signal on the basis of large-eddy simulation data. *Radio Sci.*, **34**(6), 1437–1459.
- Rogers, R. R., W. L. Ecklund, D. A. Carter, K. S. Gage, and S. A. Ethier, 1993: Research applications of a boundary-layer wind profiler. *Bull. Amer. Meteor. Soc.*, **74**(4), 567–580.
- Scipi3n, D. E., P. B. Chilson, E. Fedorovich, and R. D. Palmer, 2008: Evaluation of an LES-based Wind Profiler Simulator for Observations of a Daytime Atmospheric Convective Boundary Layer. *J. Atmos. Oceanic Technol.*, **25**, 1423–1436.
- Wilczak, J. M., E. E. Gossard, W. D. Neff, and W. L. Eberhard, 1996: Ground-based remote sensing of the atmospheric boundary layer: 25 years of progress. *Boundary-Layer Meteorol.*, **78**, 321–349.
- Yu, T.-Y., 2000: *Radar studies of the atmosphere using spatial and frequency diversity*. Ph.D. thesis, University of Nebraska, Lincoln, Nebraska.
- Zhang, G., and R. J. Doviak, 2007: Spaced-Antenna Interferometry to Measure Crossbeam Wind, Shear, and Turbulence: Theory and Formulation. *J. Atmos. Oceanic Technol.*, **64**, 791 – 805.